THE ASTROPHYSICAL JOURNAL, 250:L79–L83, 1981 November 15

EXTENDED OH MASER EMISSION FROM CIRCUMSTELLAR SHELLS AND THE ENVELOPE AROUND OH 26.5+0.6

BOUDEWIJN BAUD
Radio Astronomy Laboratory, University of California, Berkeley
Received 1981 June 15; accepted 1981 July 29

ABSTRACT

The extended diffuse component of the 1612 MHz OH maser emission from circumstellar envelopes around OH/IR stars has been studied with the VLA spectral line system. The first results show extended emission, in some cases distributed over several arc seconds, with maser line brightness temperatures of 10^4–10^6 K. The emission from OH 26.5+0.6 is considered in detail. It shows an overall velocity structure consistent with an expanding circumstellar shell model. The inner and outer radii of the masing shell are 0.4–1.1 and 4.6×10^{16} cm, respectively. Large-scale spatial asymmetries appear in the shell, with evidence for a ringlike structure seen edge-on. This structure appears to be a reflection of actual density variations within the envelope, rather than the effect of velocity crowding or of variations in the infrared pump rate. New, independent determinations result in distances for IRC +10011 and OH 26.5+0.6 of 570 and 800 pc, respectively.

Subject headings: masers — stars: circumstellar shells — stars: mass loss

I. INTRODUCTION

The strong 1612 MHz OH maser line is an excellent tracer for the structure and kinematics of extended circumstellar shells around late-type M giants and supergiants. VLBI observations of these so-called OH/IR stars reveal the existence of small (< 0.″1), bright (T_B = 10^{8-9} K) hot spots. Their distribution and kinematics usually do not show the simple, ordered behavior expected from an expanding circumstellar shell (e.g., Olnon 1977; Reid *et al.* 1977). Furthermore, in most cases more than 90% of the total emission is resolved out, even at the shortest VLBI baselines of several hundred kilometers, indicating structure on a scale of 0.″5–1″ or more (Reid *et al.* 1977; Bowers *et al.* 1980). At baselines of the order of 100 km or less, the emission shows evidence for a simple shell structure (Booth *et al.* 1981).

We have used the NRAO[1] Very Large Array spectral line system for the first time to study this extended component of the 1612 MHz OH emission from seven Mira variables and M supergiants. In this *Letter* we present the first general results. We discuss in detail the observations of OH 26.5+0.6, a prime example of an OH/IR star, which show all the microwave features typical of these objects.

II. OBSERVATIONS AND RESULTS

The observations were carried out on 1980 May 29 with six antennas covering a range of spacings from 2 to 26 km and with a spectral resolution of 7.3 kHz. The observation and calibration procedures will be discussed in more detail in a later paper. The narrow, strong emission lines caused strong spectral ringing. Because no option for smoothing the data in the spectral domain was available at the time, maps of individual channels were first Hanning smoothed to a resolution of 12.2 kHz by combining the maps from neighboring channels in the following way: $\frac{1}{4} + \frac{1}{2} + \frac{1}{4}$. This reduced the spectral sidelobe level to well below the dynamic range limit of about 2.5%. These smoothed maps were then cleaned using the conventional CLEAN procedure (Högbom 1974).

The sources are listed in Table 1. The right ascension and declination refer to the center of the emission from the extreme ends of the velocity profile. In all cases this emission from the near and far side of the envelope is unresolved or barely resolved (1″ × 2″), in agreement with the VLBI results, and spatially coincident within the uncertainties (< ±0.″3). The emission also lies within the error box of the optical or infrared stellar position. The data show no evidence for large-scale rotation in any of the sources. The shell radii have been derived using equation (1) (§ III).

The maps (see Fig. 1) suggest more or less smoothly distributed maser emission with a brightness temperature of 10^4–10^6 K, which is three orders of magnitude lower than that of the components detected in VLBI experiments. The spatial structure of the emission between the two profile peaks varies with velocity in a manner qualitatively consistent with an expanding shell: i.e., the spatial extent increases as the map velocity

[1]The National Radio Astronomy Observatory is operated by Associated Universities, Inc., under contract with the National Science Foundation.

approaches the center velocity of the star. (All radial velocities are with respect to the stellar velocity, unless stated otherwise.) The corresponding decrease in total flux implies a lower maser brightness temperature at lower velocities, which can be readily explained as a simple geometrical effect of decreasing coherent path length with decreasing velocity in an isotropically radiating medium (Reid *et al.* 1977).

VLBI measurements (Reid *et al.* 1977) are also consistent with a model of many unresolved ($\ll 1''$), high-brightness components. However, in such a model the brightness temperature *of each component* must then decrease rapidly with decreasing velocity, implying that the maser emission from each component is not isotropic but strongly beamed radially outward. Although our data do not exclude such a multicomponent model, the more simple geometrical explanation for the decreasing flux with decreasing velocity seems to favor a smooth distribution of low-brightness maser emission.

III. THE ENVELOPE AROUND OH 26.5+0.6

This optically obscured OH/IR star is one of the strongest sources of 1612 MHz OH emission. Figure 1 shows the Hanning-smoothed cross power spectrum from the shortest baseline (2 km), which is essentially equal to the total power spectrum, and maps of the independent velocity intervals separated by 2.3 km s^{-1}. Radial velocity with respect to the stellar velocity (27.1 km s^{-1}) and the maximum in the map in jansky per beam area are listed in Table 2.

In a reference frame at rest with respect to the star, the emission in a symmetrically expanding shell at a given line-of-sight velocity, v_r, originates from material in an open cone centered on the star, whose apparent angular extent is given by

$$a(v_r) = A\left[1 - \left(\frac{v_r}{v_e}\right)^2\right]^{1/2}. \quad (1)$$

A is the total angular diameter of the shell, and v_e is the shell expansion velocity (14 km s^{-1}). The highest velocity gas must originate in a narrow double cone with its axis along the line of sight through the center of expansion and should therefore reflect the stellar position. This position, deduced from the maxima in the map at 15.1 and -16.7 km s^{-1}, is indicated with a filled circle. At most velocities the star is centered on the emission, close to a local minimum (as for v_r = 6.0, 3.8, 1.5, -0.8, and -3.0 km s^{-1}) or a saddle point (10.6, 8.3, -5.3, -7.6, and -9.9 km s^{-1}). This suggests an inner shell radius between 0.4 and 1.1×10^{16} cm at a distance of 800 pc (see § V). This minimum radius is consistent with values derived by Goldreich and Scoville (1976) based on OH abundance considerations.

The maps show that the circumstellar shell exhibits large-scale asymmetries both at the near and far side. These asymmetries are further illustrated in Figure 2, where we have plotted the equivalent width extent of the main body of the emission at the 10% contour level, corrected for beam broadening, as a function of v_r. Also shown are lines of constant angular shell diameter A from equation (1). These data suggest that the emission region of the shell is thick ($> 0.5\ R_{\rm shell}$) with the near side about 50% larger than the far side. The mean outer diameter is about 8″ (9.2×10^{16} cm). A plot of the total area in the maps instead of the equivalent width extent yields similar results.

TABLE 1

OH/IR SHELL PARAMETERS

Name	R.A. (1950)[a]	Decl. (1950)[a]	V_e (km s^{-1})	Distance (pc)	Half-Intensity Shell Radius (″)	Mean Shell Radius (10^{16} cm)
IRC +10011 ...	$01^h03^m48^s.10$	+12°19′51″.5	19	570[b]	4	3.3[d]
IRC +60154 ...	05 15 06.44	+63 12 51.0	14.5	...	< 0.5	...
VY CMa	07 20 54.75	−25 40 11.8	31.5	1500	2.5	5.5
IRC −20197 ...	09 42 56.50	−21 47 54.3	12	740	< 0.5	< 0.5
VX Sgr	18 05 02.97	−22 13 55.0	19.5	500–1500	2.3	1.7–5.1
OH 1821−12 ...	18 21 16.86	−12 27 51.3	14	...	< 0.6	...
OH 26.5+0.6 ...	18 34 52.47	−05 26 36.9	14	800[b]	2.2	2.4[d]
					4[c]	4.6[c]

[a] Positional uncertainty is ±0″.3.
[b] This paper.
[c] Total extent at the 10% level.
[d] Based on the light travel time.

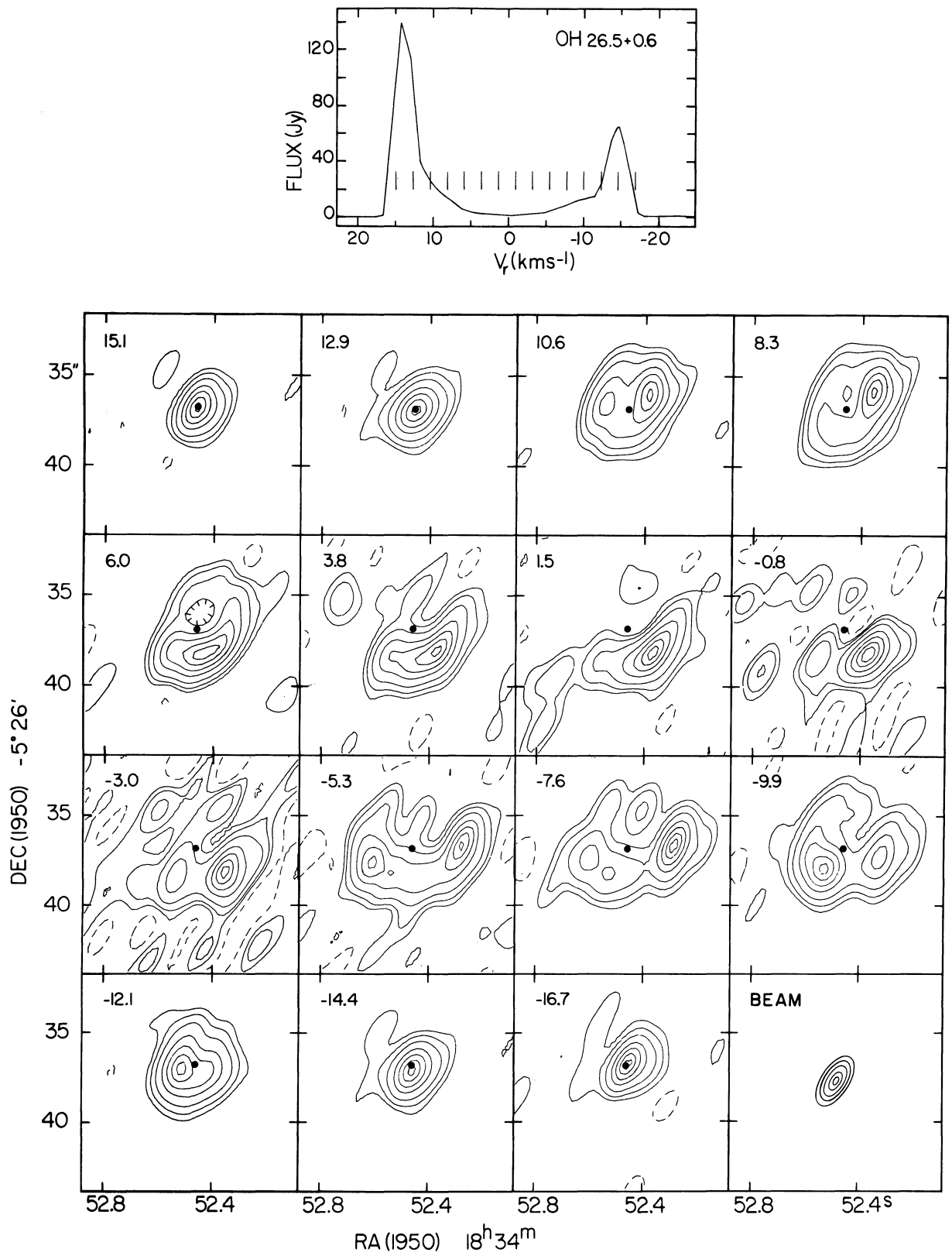

FIG. 1.—(*Top*) 1612 MHz OH cross power spectrum on a 2 km baseline. Radial velocities are with respect to the stellar velocity. Vertical bars indicate the central velocity of the maps. (*Bottom*) Maps at radial velocities noted in each frame. Contour intervals are −5, 5, 10, 20, 40, 60, 80, and 95% of the map maximum (in Table 2). The lowest contour of 2.5% has been omitted to avoid confusion in the low velocity maps. The first three intervals have been omitted in the synthesized beam. To convert to degrees Kelvin brightness temperature, multiply the contour values in Jy by 1.9×10^5 K. The dot indicates the stellar position, derived in a manner described in the text.

TABLE 2

MAP PARAMETERS FOR OH 26.5+0.6

V_r [a] (km s^{-1})	15.1	12.9	10.6	8.3	6.0	3.8	1.5	−0.8	−3.0	−5.3	−7.6	−9.9	−12.1	−14.4	−16.7
S_{peak} (Jy beam^{-1})....	38.5	53.8	7.3	4.0	1.2	0.8	0.7	0.5	0.5	0.7	2.3	2.8	8.5	34.2	1.6

[a]Velocity with respect to the stellar velocity.

Several small-scale features in the shell persist in the maps over a wide velocity range. The most prominent are the two maxima east and west of the stellar position on the near side of the shell ($v_r = -5.3$ to -12.1 km s^{-1}). A similar double feature is seen on the far side at $v_r = 10.6$ and 8.3 km s^{-1}. The separation between the two maxima appears to increase with decreasing velocity in a systematic way, suggestive of a ringlike structure that is embedded within the envelope and seen edge-on. From equation (1) we derive a mean ring radius of about 2".5 (2.9×10^{16} cm). The complete absence of similar emission at positive velocities near the stellar velocity indicates that this is only a partial ring.

IV. DENSITY STRUCTURE VERSUS VELOCITY CROWDING

Because its gain is an exponential function of the coherent path length, the maser output can be extremely sensitive to small variations in the local pump rate and density or velocity structure in the masing medium. Since most of the 35 μm pump photons are emitted from well inside the 1612 MHz maser region (Elitzur, Goldreich, and Scoville 1976), spatial variations in the pump rate are probably not responsible for the small-scale structure in the maps.

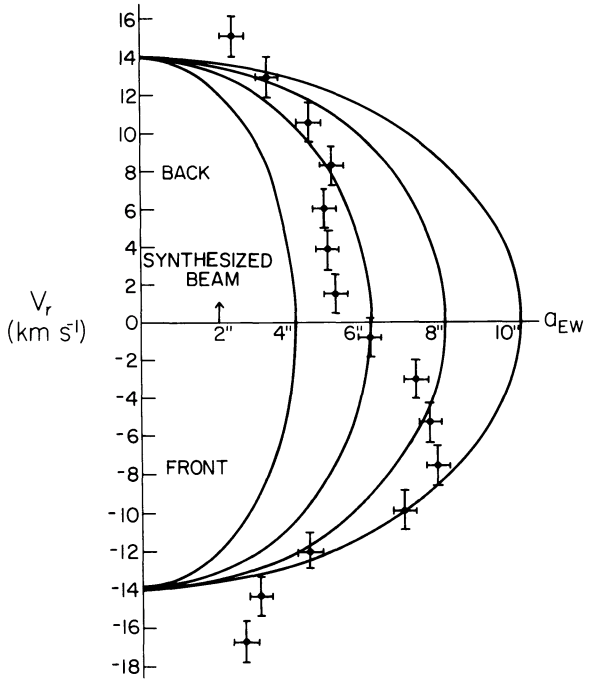

FIG. 2.—Radial velocity of OH 26.5+0.6 in the rest frame of the star vs. east-west angular extent at the 10% contour level, corrected for beam broadening. Error bars in velocity indicate the velocity width of each map. Curves of constant shell size A from eq. (1) are indicated.

Velocity crowding due to macroturbulence or streaming motions on a scale of 10^{16} cm may locally increase the coherent path length considerably and could significantly affect the map structure. An upper limit of 2 km s^{-1} to such velocity disturbances is set by the steep outer edges of the OH emission profile. If macroturbulence alone were responsible for the detailed map appearance, the emission is not expected to show any systematic structure over a velocity range larger than 2 km s^{-1}. The fact that the symmetrical double structure of the edge-on ring is seen over a velocity range of at least 7 km s^{-1} clearly indicates that macroturbulence does not play an important role. This ringlike structure would also require a rather complicated and unphysical kinematical behavior of the gas to explain it in terms of more systematic streaming motions. Hence, we conclude that most of the brightness structure must reflect density structure in the circumstellar envelope. In that case the edge-on ring structure may be due to a strongly increased mass loss rate about 700 years ago.

V. DISTANCE

Information on the angular size and the phase lag between the two line-component "light curves," which correspond to the linear size of the shell, yields an independent distance estimate for OH/IR stars (Schultz, Sherwood, and Winnberg 1978). For two objects in Table 1 phase lag information is available. Jewell, Webber, and Snyder (1980) derived a linear shell radius of $(3.3 \pm 0.7) \times 10^{16}$ cm for IRC +10011. The angular radius of 4", determined from the present data, implies a distance of 570 ± 100 pc, which is in excellent agreement with the value of 510 pc derived by Hyland *et al.* (1972), who assumed a stellar luminosity of $10^4\ L_\odot$.

In the case of OH 26.5+0.6, Herman and Habing (1981) found a linear radius of $(2.4 \pm 2) \times 10^{16}$ cm from their phase lag data. The maps in Figure 1 are dominated on the near side by the edge-on ringlike structure with a radius of 2".5 and on the far side by a single broad maximum south of the star at an angular distance of

1".9. Taking the mean values of these radii, we derive an approximate distance of 800 pc, with an uncertainty of about a factor of 2. This value is significantly smaller than the kinematical value of 2 kpc, assuming circular galactic rotation. However, OH/IR stars such as OH 26.5+0.6, with $v_e < 15$ km s^{-1}, possess large random stellar velocities of 30 km s^{-1} superposed on galactic rotation (e.g., Baud *et al.* 1981). Hence, the kinematical distance estimate is uncertain by much more than a factor of 2. We believe that the present geometrical distance determination of 800 pc, which involves fewer assumptions than the kinematical method, is a much better estimate of the actual distance to OH 26.5+0.6.

I would like to thank the VLA staff, in particular Arnold Rots and John Dreher, for their assistance in the observations and data reduction; D. Black for the measurement of the OH flux of some of the OH/IR sources; D. Backer, P. Goldreich, and A. Winnberg for useful discussions, and J. Bieging and H. Matthews for a critical reading of the manuscript. This work was funded by NSF grant AST 78-21037.

REFERENCES

Baud, B., Habing, H. J., Matthews, H. E., and Winnberg, A. 1981, *Astr. Ap.*, **95**, 165.
Booth, R. S., Kus, A. J., Norris, R. P., and Porter, N. D. 1981, *Nature*, **290**, 382.
Bowers, P. F., Reid, M. J., Johnston, K. J., Spencer, J. H., and Moran, J. M. 1980, *Ap. J.*, **242**, 1088.
Elitzur, M., Goldreich, P., and Scoville, N. 1976, *Ap. J.*, **205**, 384.
Goldreich, P., and Scoville, N. 1976, *Ap. J.*, **205**, 144.
Herman, J., and Habing, H. J. 1981, preprint.
Högbom, J. A. 1974, *Astr. Ap. Suppl.*, **15**, 417.
Hyland, A. R., Becklin, E. E., Frogel, J. A., and Neugebauer, G. 1972, *Astr. Ap.*, **16**, 204.
Jewell, P. R., Webber, J. C., and Snyder, L. E. 1980, *Ap. J. (Letters)*, **242**, L29.
Olnon, F. M. 1977, Ph.D. thesis, Leiden.
Reid, M. J., Muhleman, D. O., Moran, J. M., Johnston, K. J., and Schwartz, P. R. 1977, *Ap. J.*, **214**, 60.
Schultz, G. V., Sherwood, W. A., and Winnberg, A. 1978, *Astr. Ap. Letters*, **63**, L5.

BOUDEWIJN BAUD: Radio Astronomy Laboratory, University of California, Berkeley, CA 94720